Available online at www.sciencedirect.com
ScienceDirect
Journal of the European Ceramic Society 29 (2009) 1631–1639
www.elsevier.com/locate/jeurceramsoc

Development and characterisation of high-density oxide fibre-reinforced oxide ceramic matrix composites with improved mechanical properties

C. Kaya [a,*], F. Kaya [b], E.G. Butler [c], A.R. Boccaccini [d], K.K. Chawla [e]

[a] *Yildiz Technical University, Faculty of Chemistry and Metallurgy, Department of Metallurgical and Materials Engineering, Davutpasa Campus, Esenler, Istanbul, Turkey*
[b] *Zonguldak Karaelmas University, Engineering Faculty, Department of Metallurgical Engineering, Zonguldak, Turkey*
[c] *The University of Birmingham, IRC in Materials Processing and School of Metallurgy and Materials, Edgbaston, Bırmingham B15 2TT, UK*
[d] *Imperial College London, Department of Materials, Prince Consort Road, London SW7 2BP, UK*
[e] *University of Alabama at Birmingham, Department of Materials, Birmingham, AL 35294, USA*

Received 1 August 2008; received in revised form 23 September 2008; accepted 27 September 2008
Available online 31 December 2008

Abstract

A low cost and reliable ceramic matrix composite fabrication route has been developed. It involves the coating of 2D woven ceramic fibres (Nextel™ 720) with oxide nano-size ceramic particles by electrophoretic deposition (EPD) followed by impregnation of the coated fibres with ceramic matrix and warm pressing at 180 °C to produce the "green" component ready for pressureless sintering. The effects of two different weak interface materials, $NdPO_4$ and ZrO_2, on the thermomechanical properties of the composites are also examined. Damage mechanisms, such as debonding, fibre fracture, delamination and matrix cracking within the composite plates subjected to tensile loading are analysed using acoustic emission technique and correlated with microstructure. It is shown that the composites with $NdPO_4$ interface, 10% porosity and 40 vol.% fibre loading have superior themomechanical properties in terms of strength and damage-tolerant behaviour in multilayer plate form. The improved sinterability and microstructure stability at moderate temperatures ensure both the fibre integrity and load transfer efficiency resulting in high strength damage-tolerant composites. The final components produced are considered to be suitable for use as shroud seals and insulating plates for combustor chambers in aircraft engines.

Keywords: Ceramic composite; AL_2O_3; Nextel™ 720; Interphase; Electrophoretic deposition

1. Introduction

Ceramic matrix composites (CMCs) can display quasi-ductile deformation behaviour when mechanisms such as crack deflection, fibre pull-out, crack bridging and debonding can be made to operate by optimising the strength of the interface between fibre and matrix.[1–3] Oxide/oxide CMCs are excellent candidate components for high temperature applications due to their increased toughness, inherent oxidation resistance, good thermal shock resistance, decreased flaw sensitivity and damage-tolerant behaviour.[1–3] When CMCs are designed for high-risk and high-temperature applications, three constituents should carefully be selected and controlled for obtaining the required performance: (a) reinforcement fibres with high strength and modulus, (b) a high temperature-resistant ceramic matrix and (c) an interface that prevents occurrence of any chemical reaction between fibre and matrix.[4,5] The ceramic matrix selected should be chemically compatible with the ceramic fibres and the interface should also be compatible with both to improve the overall performance. In recent years, oxide-based composites have been the centre of many research activities as CMCs are required to be compatible with their service atmospheres which are generally oxidising, such as combustion gases.[3,6–11] After selecting the ideal matrix, interface and fibres, the most important task is to choose a viable and cost-effective processing technique for the manufacture of the final component. In the present work we have investigated the use of a novel multi-step technology that involves electrophoretic deposition (EPD) coating of woven ceramic fibres followed by impregnation of the ceramic matrix onto individual fibre mats and finally warm

* Corresponding author. Tel.: +90 2124491866; fax: +90 2124491554.
E-mail address: cngzky@yahoo.co.uk (C. Kaya).

0955-2219/$ – see front matter © 2008 Elsevier Ltd. All rights reserved.
doi:10.1016/j.jeurceramsoc.2008.09.027

pressing of the coated and impregnated fibre mats for consolidation of the composites in multilayer form. This process leads to the reduction of the overall porosity and hence to improved mechanical properties. Damage mechanisms of the optimised CMCs during tensile strength tests were analysed using in situ acoustic emission technique.

2. Experimental work

2.1. Matrix material

High purity α-alumina powder (Tai-Micron, Japan) with an average particle size of 160 nm and surface area of 14.3 m^2/g was used as the matrix material. Alumina powder was first dispersed in distilled water with the additions of dispersant, liquid binder, which is a water based acrylic polymer (Duramax B1014, Chesham Chemicals Ltd., UK), and 0.5 wt.% colloidal Y_2O_3 with an average particle size of 10 nm (Nyacol Corp., USA) as sintering aid. The suspension was magnetically stirred for 2 h followed by mechanical ball-milling with alumina balls for 8 h and finally ultrasonication for 0.5 h. The solid-loading of the suspension was 85 wt.% and the pH was adjusted to be around 4.

2.2. Interface materials

$NdPO_4$ and ZrO_2 were used as interface materials to coat the woven fibre mats using electrophoretic deposition. The techniques for the synthesis of these powders were reported in detail elsewhere.[2,8] Briefly, $NdPO_4$ was prepared by the neutral reaction of neodymium nitrate with ammonium di-hydrogen phosphate (ADPH) at room temperature. Equimolar amounts of $Nd(NO_3)_3$ and ADPH were dissolved in water to make 0.25 M solutions. The two solutions were mixed by vigorous stirring and heating, followed by filtration. The resultant gel filtrate was then dried and calcined at 1000 °C for 3 h to yield stoichiometric $NdPO_4$ monazite powder with an average particle size of 60 nm. A 15 wt.% aqueous suspension was prepared by ball milling for 4 h with the pH value adjusted to be 3. Hydrothermal processing was used to synthesise ZrO_2 powders. Zirconium acetate precursor was processed in an autoclave at 220 °C under autogeneous pressure for 2 h. The resultant sol was dried at 110 °C for 1 h and calcined at 600 °C for 4 h to remove excess acetates and obtain zirconia particles (with an average particle size of 20 nm). Zirconia particles were re-dispersed in distilled water with solid-loading of 15 wt.% and a pH value of 2.

2.3. Fibre coating by EPD

Eight-harness satin woven mullite fibre mats with 1200 single filaments in a bundle (Nextel™ 720, 3M, USA) were used as reinforcement. The fibre mats were pre-treated by desizing at 500 °C for 1 h to remove the organic protection layer from the fibre surface. The fibre mats were then immersed in an ammonia based solution, consisting of an ammonium salt of polymethacrylic acid (Versical KA21, pH:9, Allied colloids, UK) in order to create a strong negative surface charge on the fibre surface. The EPD coating cell shown in Fig. 1 was used to coat the fibre mats using an electrode separation of 20 mm and a deposition voltage of 10 V d.c. for 3 min. The coating chamber made of Perspex contains two stainless steel electrodes (30 cm × 20 cm) which are connected to a power supply. The coating suspensions ($NdPO_4$ and ZrO_2) were used separately. Coated fibre mats were then heat treated at 600 °C for 0.5 h to increase the adhesion between the fibre and the coating layer.

Fig. 1. The EPD coating unit connected to the power supply.

2.4. Composite processing

It is very important to obtain ceramic composites with the lowest possible porosity to achieve superior mechanical properties. The approach followed here to improve composite densification was to impregnate the electrophoretically coated fibres with nano-sized Al_2O_3 particles in suspension. A device was developed in which suspension flow onto the fibre mat was automatically controlled, as shown in Fig. 2a. Each coated layer of fibres is taken in turn and placed on a clean sheet of glass. A controlled amount of suspension is then poured onto the fibre mat, where upon a roller is used to ensure an even and thorough impregnation. The fibre mat is then carefully turned over and the process repeated. Once one layer has been so treated, it was carefully laid on a sheet of filter paper. The next layer of fibres was subjected to the same treatment, and then neatly stacked on top of the first layer in parallel condition. In this way the desired number of layers (12 layers in the present work to obtain 40 vol.% fibre loading in the composite) was built up. The "green bodies" containing 12 impregnated fibre mats were then stacked in a warm pressing device shown in Fig. 2b to compress and consolidate the multilayer structure at 180 °C for 2 h. To ensure that the layers of fibres would not adhere to the supports, aluminium foil was introduced below the layer of filter paper already supporting the fibres. Once the sample was fully constructed, spacers were placed at either side in order to obtain a composite thickness of 3 mm. The warm pressed specimens were finally pressureless sintered at 1200 °C for 2 h in air. The sintered composite plates were then cut to fabricate specimens for mechanical testing and microstructural observations. Fig. 3

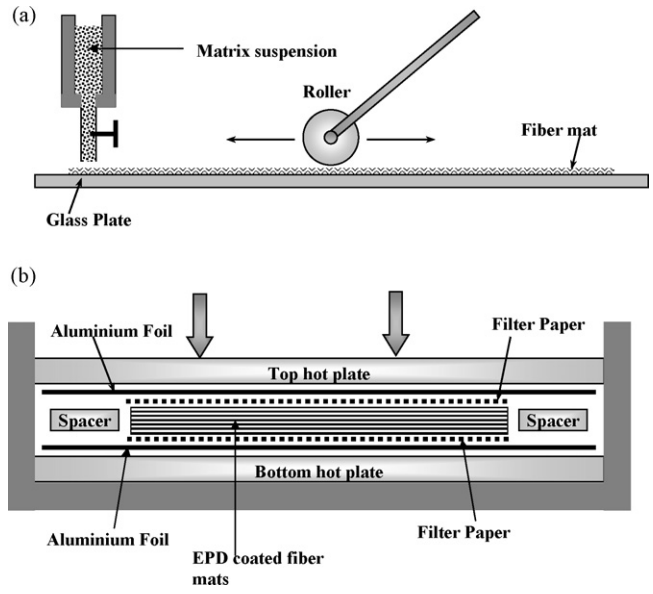

Fig. 2. Schematic representation of (a) impregnation process and (b) warm pressing for consolidation of the multilayer composite plates.

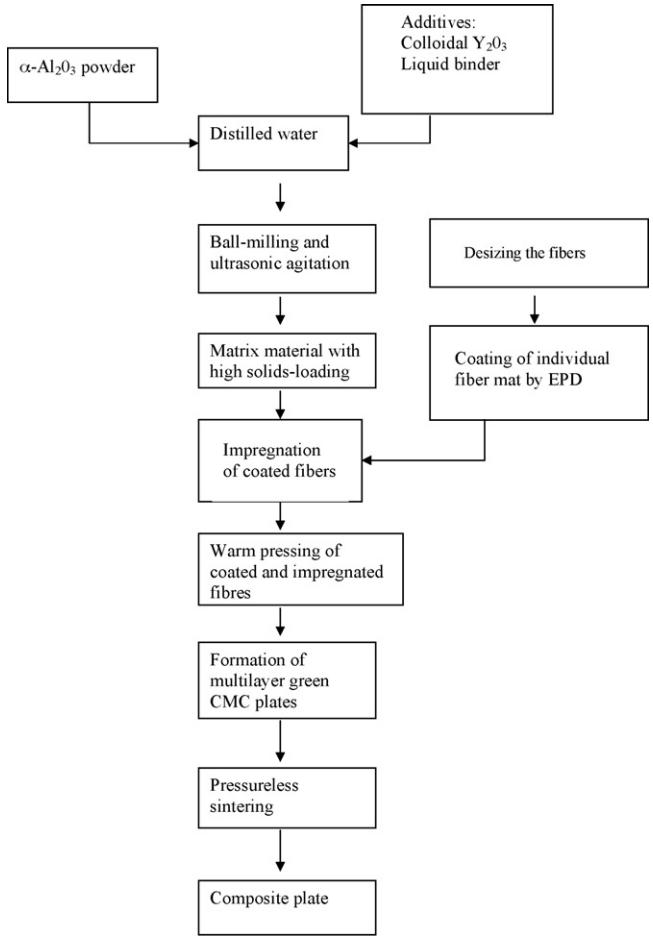

Fig. 3. Flow chart showing the manufacturing of woven mullite fibre-reinforced alumina matrix composites.

shows the manufacturing steps of the fibre-reinforced composites and Fig. 4 shows the final sintered composite plate and its microstructure.

2.5. Mechanical testing

Tensile and flexural strength test bars (50 mm × 15 mm × 3 mm and 100 mm × 10 mm × 3 mm in dimensions for flexural and tensile test bars, respectively) were cut from sintered composite panels using an Accutom 5 high-speed, precision diamond saw, and then both surfaces were ground to parallel using a 40 μm diamond resin bonded disc. All sharp edges were bevelled using 6 and 3 μm diamond pastes on soft cloths in order to minimise possible flaw sources. The tensile surfaces were then polished to a 0.25 μm finish using diamond paste. A typical tensile test specimen is shown in Fig. 5a. To enable samples to be assembled accurately, a jig was designed and manufactured as shown in Fig. 5b. It is important that the samples be fixed and aligned correctly as the load must be applied along the centreline, otherwise shear forces will distort the results (see Fig. 5c). The jig uses two steel pins to align the plates, with a small macralon block to centre the sample. Spacers are also required to keep the steel plates apart the correct distance. Room- and high-temperature four-point bend tests (test bars with dimensions 50 mm × 15 mm × 3 mm) were performed on an Instron Testing machine fitted with a furnace which had tungsten mesh elements, which enabled the tests to be carried out at temperatures up to 1500 °C. The pushrods and fixtures are all made from a tungsten–zirconium–molybdenum alloy. Specimens to be tested at 1300 °C were held at the test temperature for at least 1 h prior to the testing to allow the system to equilibrate and to ensure that the specimen was at this temperature. Tensile tests were performed at room temperature. For flexural and tensile tests, a constant cross-head speed of 0.5 mm/min. was used. The interlaminar shear strength of the coated and impregnated layers was also determined using the test specimen geometry shown in Fig. 6. In order to measure the bonding strength between fibre mats, individually coated and impregnated mats were sintered together using exactly the same cycle used for the composite itself and a tensile test specimen, as shown in Fig. 6, was prepared. The Perspex plates used for alignment were strongly glued (Epoxy adhesive, Good Fellow, UK) to the fibre and the aluminium tap surfaces using adhesives that provide a very strong adhesion so that only the bonding strength could be measured during the tensile test. For all mechanical property results reported, seven samples were used for each reported value by eliminating the highest and the lowest values (to obtain more reliable data and eliminate big variations) and taking the average value of the remaining five values.

2.6. Acoustic emission monitoring

The location of sensors and the experimental design for acoustic emission monitoring are shown in Fig. 7. Acoustic emission (AE) is a non-destructive technique (NDT) based on elastic waves generated by the rapid release of localised sources like transient relaxation of stress and strain fields. Plas-

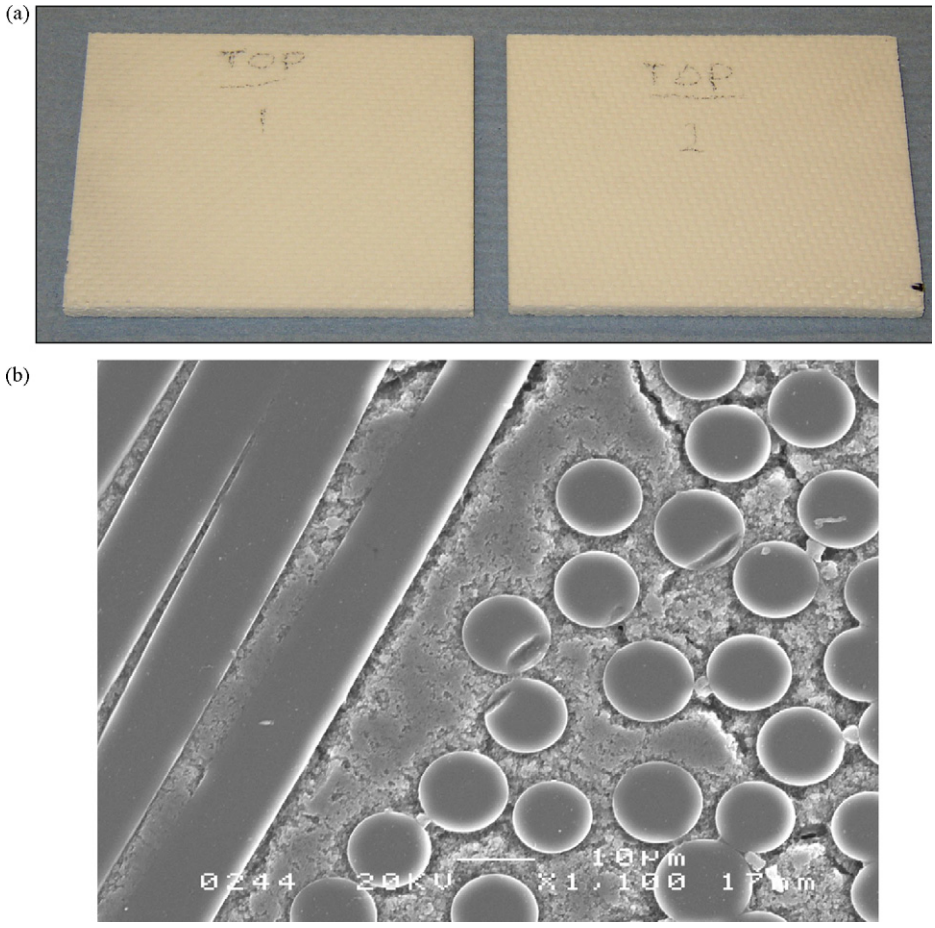

Fig. 4. (a) An optical microscopy photo of the woven mullite fibre (Nextel 720™) reinforced alumina matrix composite with $NdPO_4$ interface and (b) SEM image of the same plate indicating the detailed microstructure.

tic deformation, crack initiation and growth as well as fracture events result in AE signals. Depending on the nature of energy release, two types of AE response are observed; continuous and burst. Continuous AE signals are characterised by low amplitude while burst type AE signals are characterised by high amplitude pulses. Continuous type signals are caused by plastic deformation, diffusion controlled phase transformations, while burst type signals are caused by diffusionless phase transformations, crack initiation and propagation. However it is difficult to use a single all-encompassing parameter to describe an experimental result uniquely. Some of the parameters used for identification of source are; amplitude, energy level, duration and rise time.[13] AE has been used extensively in composite materials characterisation in order to identify the possible mechanism of fracture.[14,15] It is reported that AE sources such as matrix cracking, fibre/matrix interfacial separation and fibre failure could be evaluated simultaneously in both metallic and ceramic matrix composites.[14–19] The elastic wave generated by the propagation of a crack through the solid to the surface can be recorded by one or more sensors. The sensor is a transducer that converts the mechanical wave into an electric signal. In this way information about the existence and location of a crack can be obtained. A variety of damage mechanisms including matrix cracking, fibre debonding and fibre fracture, which are common events when a ceramic composite is subjected to loading, can be identified[19] As damage progresses, different forms of AE signals are detected depending on the type of fracture mechanism acting.

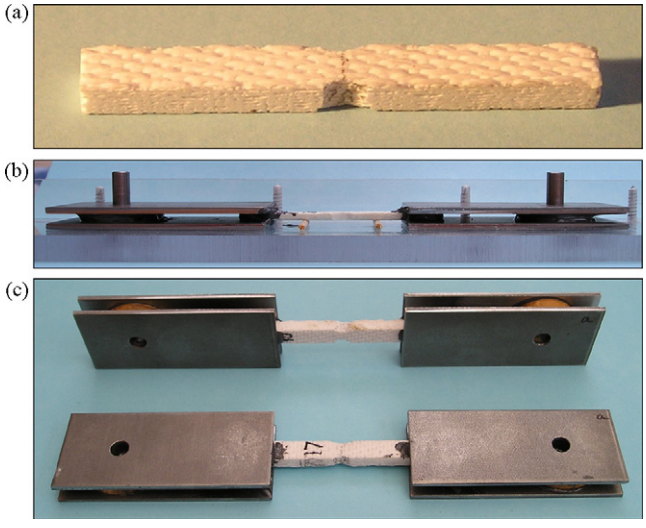

Fig. 5. Images of (a) tensile test specimen, (b) jig used for alignment and (c) aligned test specimen.

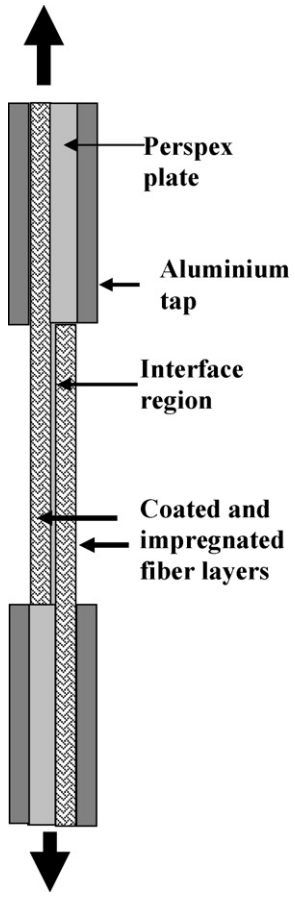

Fig. 6. Schematic representation of the test sample arrangement to measure the interlaminar shear strength (bonding strength) between two fibre mats.

2.7. Microstructural characterisation

Microstructural examinations were carried out on sintered composite samples using a high-resolution Field Emission Gun (FEG) SEM (FX-4000, Jeol Ltd., Japan). More detailed observations were made using transmission electron microscopy (TEM, Jeol Ltd., Japan, 4000 FX TEM) operated at 400 kV, and equipped with an energy dispersive X-ray (EDX) analysis unit. Porosity and pore size were measured using a mercury porosimeter (Hg Por, Micromechanics Instrument Corp., USA) using a penetrometer weight of 62.79 g, and penetration volume of 6.188 mL. The Archimedes' technique was used for density measurements.

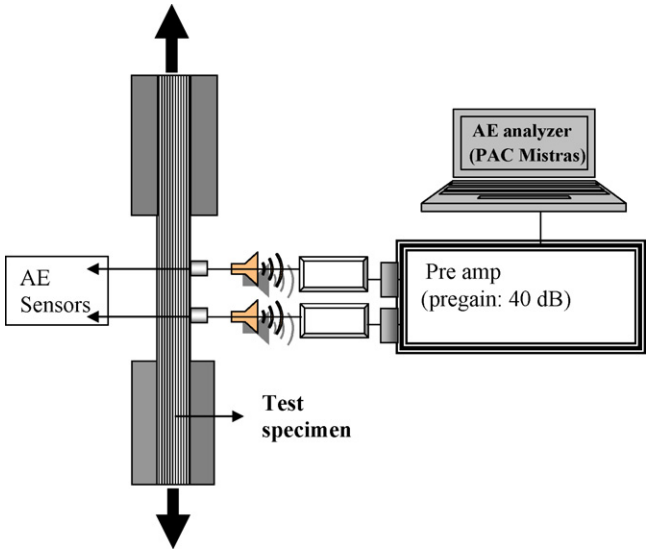

Fig. 7. Schematic representation of experimental set up for acoustic monitoring during tensile test.

3. Results and discussion

An optical microscopy image of the composite plates produced after pressureless sintering at 1200 °C for 2 h is shown in Fig. 4a indicating that a homogeneous and macro-flaw free surface structure of the plate was obtained. The final component shown in Fig. 4a contains 12 layers with a fibre volume fraction of 40%. The overall thickness of the plate was ~3 mm and no delamination of the layers was observed after sintering. The final sintered microstructure of the composite shown in Fig. 4b contains 10–14 vol.% porosity which is quite low for this type of composite systems. The development of complex and highly sinterable matrix precursors which are silica free, comprising nano-scale alumina powders dispersed in aqueous solution mixed with nano-size colloidal Y_2O_3, led to full infiltration by the impregnation technique, as shown in Fig. 4b. It can be concluded that the matrix precursors developed display favourable rheological properties during both the impregnation and warm pressing stages resulting in enhanced matrix infiltration and formability. In our previous research[2,7] using a combination of EPD and pressure filtration for different composite systems, for example mullite/mullite CMCs, a successful deposition was also achieved leading to manufacture of sintered samples with porosity levels from 15 to 20%. The present work represents an advance in the development of CMCs with lower porosity using an impregnation technique combined with warm pressing. It is expected from these results that improved sinterability and stability at moderate temperatures will ensure continued fibre integrity and matrix load translation efficiency resulting in high strength, damage-tolerant CMCs. Selected properties of the composite plates produced are given in Table 1. As shown in this table, using two different interface materials, namely $NdPO_4$ and ZrO_2, quite similar mechanical properties were obtained at room temperature (four-point bending strength values of 279 and 260 MPa and tensile strength of 142 and 136 MPa, respectively). However, when the samples were subjected to bend strength test at 1300 °C, only a 5% reduction in strength was recorded for composites with $NdPO_4$ interfaces (from 279 to 266 MPa) whereas over a 10% decrease was measured for composites with ZrO_2 interfaces (from 260 to 232 MPa). Although these two interface materials are known to be compatible with the matrix and fibres used, the difference in strength is most probably related to the possible different microstructure of the interface at high temperature. Load–displacement curves of the composite samples with the two interfaces were also recorded for comparison at room and high temperatures (1300 °C), as shown in Fig. 8. As shown in Fig. 8a, both composites exhibit

Table 1
The effects of interface materials on the properties of ceramic composite tested.

Interface material	Four-point bending strength, MPa	Tensile strength, (RT) MPa	Interlaminar shear strength, MPa	Average pore size, nm
$NdPO_4$	279 (RT), 266 (1300 °C)	142	9.4	80
ZrO_2	266 (RT), 232 (1300 °C)	136	8.6	70

a damage-tolerant behaviour at room temperature and composite failure started with fibre failure followed by multiple matrix cracking (the first and second peaks as arrowed in the graphs) and eventually delamination and fibre pull-out took place. Similar results were observed on the samples tested at 1300 °C, as shown in Fig. 8b, confirming that the composite plates produced in the present work showed damage-tolerant behaviour at both room temperature and at 1300 °C. The greater loss in strength at high temperature in composites with zirconia interface was attributed to the lower oxidation protection at high temperature offered by zirconia in comparison to $NdPO_4$, which does not prevent oxygen diffusion through the interface layer. For example, the density of the coating layer may play a role at high temperatures. Further experiments are now underway to clarify this behaviour and determine the possible reasons for it. It is important to avoid the occurrence of any reaction between the coating layer and the reinforcement fibres in order to obtain ideal damage-tolerant behaviour by activation of crack deflection and fibre debonding/pull-out mechanisms. To observe the interface region of a composite sample containing $NdPO_4$ interface in detail transmission electron microscopy observations were carried out. It is seen in Fig. 9 that there is no reaction zone between $NdPO_4$ and alumina matrix, the interface region is clean as evident by the absence of reaction products, which was confirmed also by TEM EDX. It is also seen from the TEM micrograph in Fig. 9 that the grain size of the $NdPO_4$ interface is about 200 nm which should act as a dense barrier preventing oxygen diffusion from the matrix through the fibres.

Table 1 also shows that tensile strength values of the composite plates with zirconia and $NdPO_4$ interphases are 136 and 142 MPa, respectively. It is also shown in Table 1 that interlaminar shear strength values are 8.6 and 9.4 MPa for the coated and impregnated fibre samples with zirconia and $NdPO_4$ interphase, respectively. These results represent a significant improvement of the present woven fibre-reinforced CMCs, which exhibit better mechanical properties in terms of room temperature tensile strength and interfacial bonding strength than previously developed composites.[2] The tensile strength and interlaminar shear strength are both improved by the addition of liquid binders

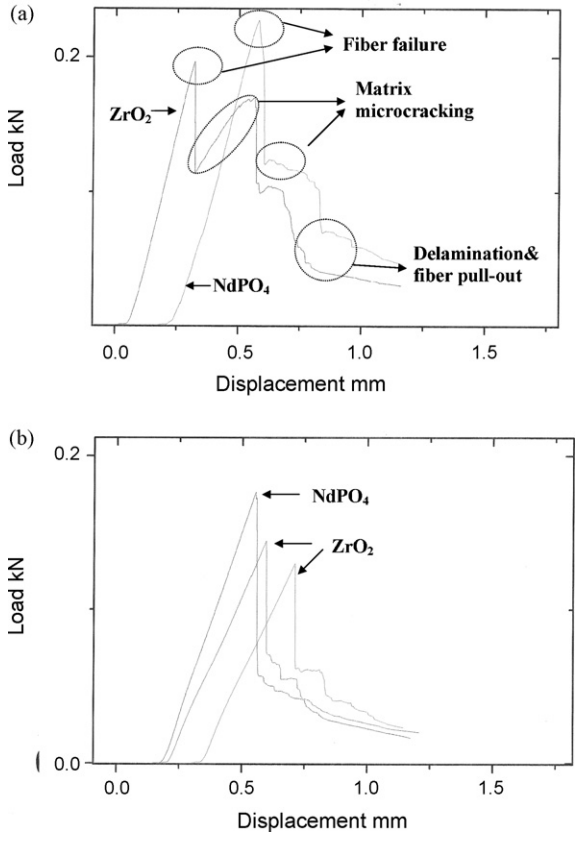

Fig. 8. Load–displacement curves of composites with zirconia and $NdPO_4$ interfaces: (a) at room temperature and (b) at 1300 °C.

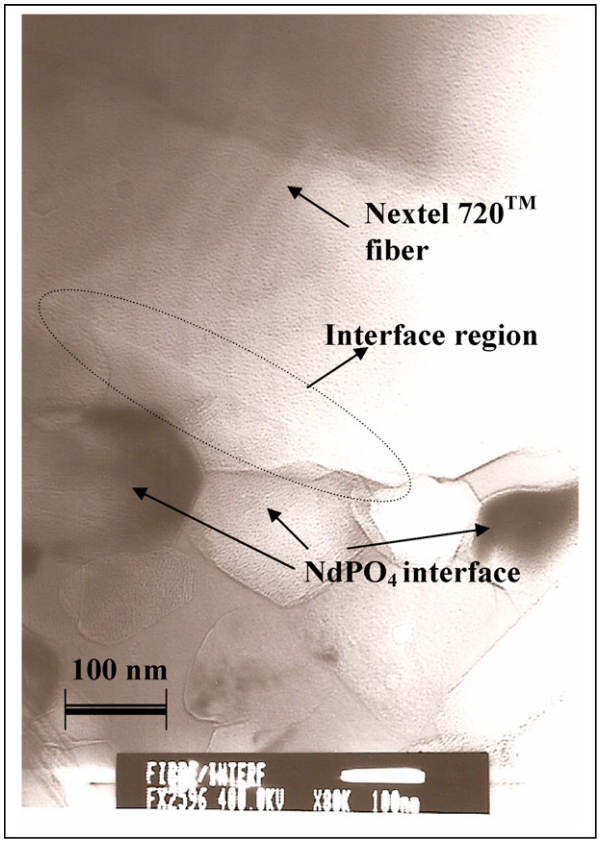

Fig. 9. Transmission electron microscopy (TEM) image of the composite sample containing $NdPO_4$ interface indicating that there is no reaction between the interface and the fibre.

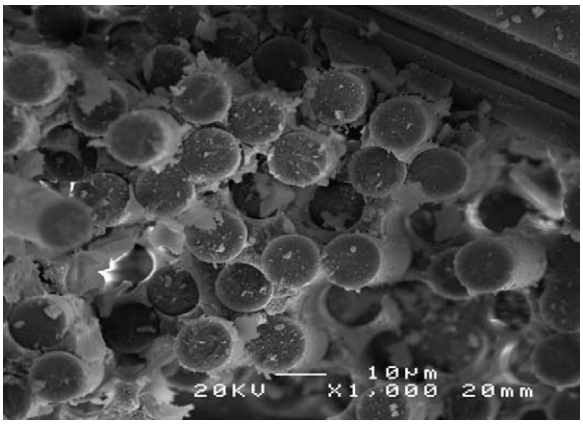

Fig. 10. FEG SEM micrograph of a composite specimen with $NdPO_4$ interface tested under tensile loading.

and nano-size colloidal yttria that have promoted the sintering kinetics of the matrix resulting in higher density values.

In our previous studies on CMCs with different oxide matrices,[2,8] the mechanical properties of the final components have been linked to microstructural variations without considering in detail the possible effects of matrix pore size on the properties. In the present work, the average pore size was measured and found to be smaller than 100 nm for composites with two different interphases, as shown in Table 1. This fine porosity is related to the presence of ultrafine yttria particles (10 nm) within the matrix that act as sintering additives and provide a more homogeneous matrix structure in terms of density and pore size distribution.

A fractured surface of a composite sample subjected to tensile test at room temperature is shown in Fig. 10 indicating the presence of extensive fibre pull-out due to mechanisms, such as fibre/matrix debonding and crack deflection both initiated by the nature of the $NdPO_4$ weak interface.

Fig. 11 shows a detailed examination of AE parameters of energy versus event duration. A distinct tail at energy values higher than $100\,J \times 10^{-18}$ and event duration higher than 1000 μs can be seen clearly. The AE events giving rise to the tail could be interpreted as fibre fractures because the fracture energy generated by high strength and high modulus fibres is expected

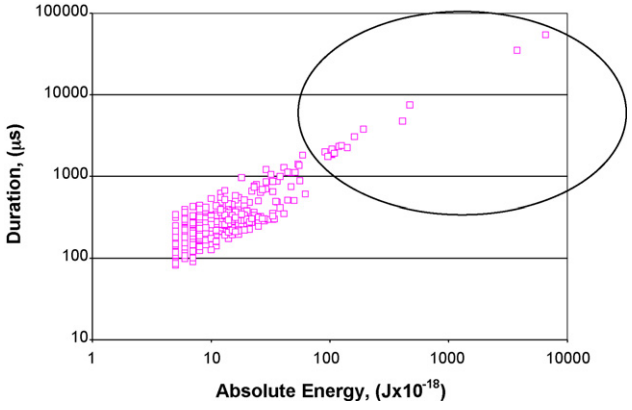

Fig. 11. AE events of the composite subjected to tensile test showing the relationship between duration and absolute energy.

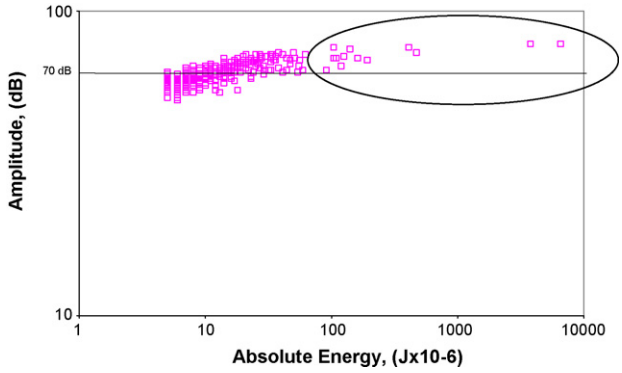

Fig. 12. AE events of the composite subjected to tensile test showing the relationship between amplitude and absolute energy.

to be higher than the energy generated by the ceramic matrix. A closer examination of AE events shows that these high energy AE events also have amplitude higher than 70 dB, as shown in Fig. 12. Both energy and amplitude level of the AE signal indicate how much energy is released during the fracture process, hence pointing to high strength-high stiffness materials such as ceramic fibres. In total fourteen events have been detected with a combination of high energy-amplitude and duration values (see Figs. 11 and 12). Two of these events significantly differ from the others as they have 100 times higher energy and duration values with the highest amplitude (78 dB) recorded during the test. These two AE events correspond to final failure. Other 12 AE events with a combination of high energy-duration and amplitude levels could be interpreted as the fracture of 12 fibre mats within the composite.

Further analysis of high amplitude (≥70 dB) events shows that there is a group of AE events with high amplitude and low energy and duration values as shown in Fig. 12. The energy values of these AE events range between 20 and $60\,J \times 10^{-18}$ with event duration between 300 and 600 μs. These groups of events could be deduced to be individual fibre fractures within the fibre mats. The ultimate tensile strength of these fibres could have been decreased (compared to the average tensile strength) due to damage occurred during processing. Other AE events are categorised as matrix related events that possibly arise from matrix cracking but also from interfacial failure.

When all AE activity is plotted against the total time of test (i.e., the extension of sample), it can be clearly seen that fibre mats fail towards the end of the tensile loading, whereas matrix related events occur throughout the test, as shown in Fig. 13. This is a clear indication of damage-tolerant behaviour of the ceramic composites. In this composite system, the fibre mat has been treated to obtain a weak interfacial strength between the ceramic fibre and matrix. AE response shows that while the matrix crack propagates fibre mats stay intact in the crack wake leading to fibre bridging, which leads to increased fracture toughness. Although some individual fibre failures were observed, these did not compromise the overall integrity of the composite. It was also seen that when one fibre mat failed due to increased load transfer from the fractured ceramic matrix, other mats also failed simultaneously within a fraction of a second.

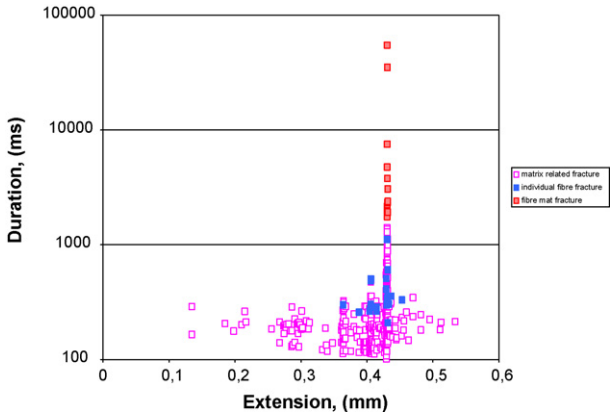

Fig. 13. AE events of the composite subjected to tensile test showing the relationship between duration and extension.

Further proof of fibre bridging can be seen in the fractography where exposed fibre ends indicate interfacial debonding and crack front deviation due to weak interfacial strength (see Fig. 10).

As a conclusion from the results presented Figs. 11–13, AE is confirmed to be a powerful NDT technique for ceramic composite characterisation providing that it is used in conjunction with other evaluation techniques, such as fractography, in order to draw a more complete picture of the relevant fracture mechanisms. Different fracture mechanisms such as matrix fracture and fibre failure could be identified using AE event parameters of energy, amplitude and duration. The identification of failure mechanisms such as interfacial separation could be rather difficult as the low energy released by such a weak source could be easily masked by the AE burst caused by fracturing fibres. AE results indicate that the fracture of these oxide matrix composites started with matrix crack initiation and propagation. Although a few individual fibre fractures were detected the majority of fibres did not fail until the final failure. Particularly, the fibre mats did not fail until the peak load was reached indicating the fibre bundles within the fibre mats stayed intact in the crack wake. This behaviour is attributed to the weak interfacial strength and fibre bridging, which in turn increases the toughness of the composite.

Overall, the present investigation has shown the development of an optimised and reproducible CMC fabrication route through understanding the relationship between matrix precursor chemistry, process parameters and final mechanical properties. The key to attain optimum mechanical properties in Nextel 720^{TM} fibre-reinforced alumina ceramic matrix composites with $NdPO_4$ interface is the development of a strong and dense matrix capable of efficient load transfer between reinforcement fibres in conjunction with retention of fibre properties after processing. The requirement for high integrity matrices can lead to fibre degradation due to high sintering temperatures necessary to achieve high densification overcoming back stresses imposed by the fibres. In the past, the addition of silica to alumina matrices as sintering aid has resulted in loss of high temperature mechanical properties, in particular time dependant properties (creep and fatigue), even at moderate temperatures (1100 °C).[12] The innovative approach to matrix formulation adopted in the present work results in a sinteractive alumina with the addition of ultra-fine particles to promote sintering kinetics and avoiding the use of other detrimental sintering aids like silica. Electrophoretic deposition coating of 2D fibre mats with nano-sized particles was successfully applied and coated samples were fully impregnated with alumina matrix using low temperature warm pressing leading to formation of damage-tolerant CMCs with superior properties. The effectiveness of this new approach is evidenced in the outstanding properties achieved (flexural strengths of 279 and 266 MPa at room temperature and at 1300 °C, respectively, in four-point bending test and a room temperature tensile strength of 142 MPa for the composite samples containing 40 vol.% fibre loading, $NdPO_4$ interface and an overall porosity of 10%). In addition, as a significant improvement, interlaminar shear strength of the multilayer composites was also improved to over 9 MPa compared to the value of 4 MPa obtained in our previous studies.[12] Currently, thermomechanical properties in terms of creep and fatigue behaviour as well as ballistic impact and fracture toughness are under investigation. Based on the properties obtained, these composites could be candidate for use as shroud seals or insulating layers for combustor chambers in aircraft engines.

4. Conclusions

Nextel 720^{TM} fibre-reinforced alumina matrix composites with two different interface materials ($NdPO_4$ and ZrO_2) were manufactured using electrophoretic deposition, colloidal infiltration and subsequent warm pressing at 180 °C to consolidate a green body in multilayer form. After pressureless sintering at 1200 °C for 2 h, the final composite had 40 vol.% fibre and 10% porosity with an average pore size smaller than 100 nm. The samples with dense $NdPO_4$ coating layer showed damage-tolerant fracture behaviour at room temperature and at 1300 °C during flexural strength test. Interlaminar shear strength of the CMC samples was determined to be over 9 MPa with a tensile strength of 142 MPa. AE results indicated that fracture of the composite started with matrix crack initiation and propagation. Although a few individual fibre fractures were detected the majority of fibres did not fail until the final composite failure. Specifically, the fibre mats did not fail until the peak load was attained indicating that the fibre bundles within the fibre mats stayed intact in the crack wake. This is due to the low interfacial strength and results in fibre bridging, which should increase the toughness of the composite.

Acknowledgements

TUBITAK (Turkish Science and Technological Research Council), EU Commission and Yıldız Technical University of Istanbul are acknowledged for financial support. Richard Brown is acknowledged for some parts of the experimental work.

References

1. Chawla, K. K., *Ceramic Matrix Composites* (*2nd ed.*). Kluwer Academic Press, Boston, USA, 2003.
2. Kaya, C., Butler, E. G., Selcuk, A., Boccaccini, A. R. and Lewis, M. H., Mullite (NextelTM 720) fibre-reinforced mullite matrix composites exhibiting favourable thermomechanical properties. *J. Eur. Ceram. Soc.*, 2002, **22**(13), 2333–2342.
3. Chawla, K. K., Coffin, C. and Xu, Z. R., Interface engineering in oxide fibre/oxide matrix composites. *Int. Mater. Rev.*, 2000, **45**, 165–189.
4. Lewis, M. H., Tye, E., Butler, E. G. and Doleman, P. A., Oxide CMCs: interphase synthesis and novel fibre development. *J. Eur. Ceram. Soc.*, 2000, **20**, 639644.
5. Warren, R. and Deng, S., Continuous fibre reinforced ceramic composites for very high temperatures. *Silicates Ind.*, 1996, **5**(6), 96–107.
6. Kanka, B. and Schneider, H., Aluminosilicate fiber/mullite matrix composites with favorable high-temperature properties. *J. Eur. Ceram. Soc.*, 2000, **20**, 619–623.
7. Kaya, C., Gu, X., Al-Dawery, I. and Butler, E. G., Microstructural development of woven mullite fibre-reinforced mullite ceramic matrix composites by infiltration processing. *Sci. Technol. Adv. Mater.*, 2002, **3**(1), 35–44.
8. Kaya, C., He, J. Y., Gu, X. and Butler, E. G., Nanostructured ceramic powders by hydrothermal synthesis and their applications. *Micropor. Mesopor. Mater.*, 2002, **54**(1–2), 37–49.
9. Stoll, E., Mahr, P., Kruger, H. G., Kern, H., Thomas, B. J. C. and Boccaccini, A. R., Fabrication technologies for oxide-oxide ceramic matrix composites based on electrophoretic deposition. *J. Eur. Ceram. Soc.*, 2006, **26**(9), 1567–1576.
10. Ruggles-Wrenn, M. B., Siegert, G. T. and Baek, S. S., Creep behavior of Nextel(TM) 720/alumina ceramic composite with +/− 45 degrees fiber orientation at 1200 degrees C. *Comp. Sci. Technol.*, 2008, **6**, 1588–1595.
11. Boccaccini, A. R., Kaya, C. and Chawla, K. K., Use of electrophoretic deposition in the processing of fibre reinforced ceramic and glass matrix composites. A review. *Compos. Part A*, 2001, **32**, 997–1006.
12. Kaya, C. and Butler, E. G., IRC Internal Report on Development of CMC. The University of Birmingham, February 2002.
13. Raj, B., Jayakumar, T. and Thavasimuthu, M., *Practical Nondestructive Testing*. Woodhead Publishing, 2002, pp. 100–105.
14. Kaya, C., Kaya, F. and Mori, H., Non-destructive damage evaluation of cyclic-fatigued alumina fiber-reinforced mullite ceramic matrix composites using forced resonance and acoustic emission techniques. *J. Mater. Sci. Lett.*, 2002, **21**, 1333–1335.
15. Kaya, C., Kaya, F. and Mori, H., Damage assessment of alumina fibre-reinforced mullite ceramic matrix composites subjected to cyclic fatigue at ambient and elevated temperatures. *J. Eur. Ceram. Soc.*, 2002, **22**(4), 447–452.
16. Kaya, F., Damage assessment of oxide fibre reinforced oxide ceramic matrix composites using acoustic emission. *Ceram. Inter.*, 2007, **33**, 279–284.
17. Kaya, F. and Bowen, P., Effect of increased interfacial strength on the fatigue crack growth resistance and crack opening displacement of β Ti 21S/SCS 6 composites. *Mater. Sci. Eng. A.*, 2008, **476**, 301–307.
18. Kaya, F., Bowen, P. and Liu, J., In-situ observation of crack opening displacement (COD) in a metastable β titanium composites. *J. Mater. Sci.*, 2008, **43**, 270–280.
19. Boccaccini, A. R., Kern, H. and Dlouhy, I., Determining the fracture resistance of fibre reinforced glass matrix composites by means of the Chevron-Notched Flexural Technique. *Mater. Sci. Eng. A*, 2001, **308**, 111–117.